Smart Structures and Systems, *Vol. 23, No. 3 (2019) 243-261*
DOI: https://doi.org/10.12989/sss.2019.23.3.243

Optimization of LQR method for the active control of seismically excited structures

Behrang Moghaddasie*[1] and Ali Jalaeefar[2]

[1]*Department of Civil Engineering, Ferdowsi University of Mashhad, P.O. Box 91775-1111, Mashhad, Iran*
[2]*Department of Civil Engineering, North Tehran Branch, Islamic Azad University, Tehran, Iran*

(Received June 24, 2018, Revised January 17, 2019, Accepted January 19, 2019)

Abstract. This paper introduces an appropriate technique to estimate the weighting matrices used in the linear quadratic regulator (LQR) method for active structural control. For this purpose, a parameter is defined to regulate the relationship between the structural energy and control force. The optimum value of the regulating parameter, is determined for single degree of freedom (SDOF) systems under seismic excitations. In addition, the suggested technique is generalized for multiple degrees of freedom (MDOF) active control systems. Numerical examples demonstrate the robustness of the proposed method for controlled buildings under a wide range of seismic excitations.

Keywords: active control; LQR method; weighting matrices; seismic excitation; modal space

1. Introduction

To protect civil structures against earthquakes and wind loads, smart structural systems can be applied to absorb destructive energy, and subsequently reduce the response of the structure (Cheng *et al.* 2010). In recent years, passive, active, semi-active and hybrid control systems are used in a number of building structures and towers (Spencer Jr. and Sain 1997, Soong and Spencer Jr. 2000, Spencer Jr. and Nagarajaiah 2003, Morales-Beltran and Paul 2015). Each control system has its own advantages and disadvantages. Based on the type and performance of the supposed structure, many efficient actuators, dampers and other control devices are designed and manufactured (Symans and Constantinou 1999, Datta 2003, Fisco and Adeli 2011, Fisco and Adeli 2011). In active control systems, control forces are determined and simultaneously applied to the structure during dynamical loadings; however, a large amount of external power is required in comparison with other control systems.

Various active control algorithms have been investigated in the literature (Soong 1988, Korkmaz 2011). Linear quadratic regulator (LQR) (Gluck *et al.* 1996, Alavinasab *et al.* 2006, Reinhorn *et al.* 2009, Miyamoto *et al.* 2016), linear quadratic Gaussian (LQG) (Lu *et al.* 1998, Song *et al.* 2006), H2- and H∞-based (Chase and Smith 1996, Yang *et al*. 2003, Li and Adeli 2016, Shukla *et al*. 2016), fuzzy control (Bani-Hani and Ghaboussi 1998, Kim and Yun 2000, Park and Ok 2015, Braz-César and Barros 2018), neural network-based (Chang *et al*. 2012), wavelet-based (Amini *et al.* 2013, Wang and Adeli 2015, Hashemi *et al.* 2016), instantaneous optimal control (Akhiev *et al.* 2002, Bahar *et al.* 2003, Tarantino *et al*. 2004) and pole assignment (Lynch and Law 2002, Amini and Samani 2014) are examples of control algorithms. On the other hand, the control scheme can be categorized in open-loop, closed-loop and closed-open-loop controls (Cheng *et al.* 2010). In the open-loop scheme, the control force of actuators is determined by a feedback of external structural excitations (such as seismic ground motion), while the response of the structure specifies the control force in the closed-loop control. The closed-open-loop scheme is a combination of both open and closed-loop. The classical open-loop and closed-open-loop control algorithm are not applicable to structures subjected to seismic excitations, since the time history of ground motion is not known a priori (Aldemir and Bakioglu 2001, Bakioglu and Aldemir 2001, Lee *et al.* 2008, Aldemir *et al.* 2012). This deficiency can be made up through applying advanced control methods (Aldemir *et al.* 2001, Yamada and Kobori 2001, Ma and Yang 2004, Aldemir 2009).

The LQR method is widely used in structural control systems (Lynch and Law 2002, Alavinasab *et al*. 2006), and its efficiency in practical applications has been proven in comparison with other advanced control algorithms (Soong *et al.* 1991, Reinhorn *et al.* 1993, Reinhorn *et al.* 2009). In this method, a weighted balance between the structural responses and control forces is kept while the structure is excited by external forces. Based on the objectives defined in the design of structural control system, weighting matrices are chosen to obtain a better performance in the seismic behavior of the structure. Although researchers have made effort to develop a systematic approach in tuning the weighting matrices (Miller *et al.* 1988, Xing *et al.* 2000, Min *et al.* 2003), there is no general solution in this context (Bahar *et al.* 2003, Aldemir *et al.* 2012). Therefore, the weighting matrices are commonly estimated by trial and error procedures (Bahar *et al.* 2003). Recently, in engineering problems, the Bayesian optimization is applied

∗Corresponding author, Ph.D.
E-mail: behrang.moghaddasie@mail.um.ac.ir

http://www.techno-press.com/journals/sss&subpage=7
ISSN: 1738-1584 (Print), 1738-1991 (Online)

to find suitable weighting matrices through a Gaussian process (Marco *et al.* 2016, Miyamoto *et al.* 2018). This method is iterative and should be used for each problem, separately. Consequently, the mentioned control approach would *not* work properly for a structure under various and unknown dynamical loadings (e.g., winds and earthquakes).

Depending on the capacity of applied active actuators and the intensity of expected excitations, the LQR method can be regulated. In the case of seismic excitations, the ground motion is not known in advance. Consequently, the required control force may exceed the actuator capacity while earthquakes happen. In this state, the active control force would remain constant at the maximum level that can be provided by the actuator, until the value of the required control force returns to the range of the actuator capacity (Miller *et al.* 1988, Xing *et al*. 2000, Min *et al*. 2003, Alavinasab *et al.* 2006). This process may excessively occur during a seismic excitation and can affect the performance of LQR method. The aim of this paper is to introduce an appropriate technique to improve the efficiency of LQR method for the active control of seismically excited structures. In this way, the uncontrolled responses of 395 single degree of freedom (SDOF) structures (with various natural periods and damping ratios) under eight different earthquakes are obtained. Then, an active control system governed by the LQR method is added to the supposed structures. In order to adjust the relationship between the values of weighting matrices used in LQR, a regulating parameter is defined. For each active control system with different maximum control forces, the optimum regulating parameter is estimated by a trial and error procedure. Here, the ratio of the maximum controlled displacement to the uncontrolled one is chosen as the performance evaluation index. Over 700,000 analyses have been done for all SDOF structures. Afterwards, the authors provide a formula to estimate the regulating parameter as a function of the natural period, damping ratio and maximum control force. It will be shown that the error caused by this estimation is small and can be neglected. Additionally, the suggested approach is generalized for multiple degrees of freedom (MDOF) structures including one or more active actuators. For this purpose, the governing equations are transformed into a modal space. Then, a combination of regulating parameters relative to each single mode is proposed to adjust the LQR method for MDOF controlled structures. Numerical examples show the efficiency of the suggested approach for a wide range of seismically excited shear-type buildings. Note that some issues, such as considering the effect of time-delay (Chung *et al.* 1995, Guoping and Jinzhi 2002, Pnevmatikos and Gantes 2011, Jang *et al.* 2014, Teng *et al*. 2016), structural nonlinearities (Wong and Hart 1997, Ohtori *et al.* 2004, Sajeeb *et al.* 2007, Materazzi and Ubertini 2012) and the existence of uncertainties in controlled structures (Mariani and Venini 1998, Wang 2003, Amini and Vahdani 2008), are beyond the scope of this research.

A brief outline of the paper is as follows: Section 2 describes the LQR method. In addition, the equation of motion and the quadratic performance measure are investigated. In Section 3, the proposed method is introduced. For this purpose, first, the optimal weighting matrices for SDOF controlled systems under seismic excitations are obtained by a trial and error procedure. Then, the method is generalized for MDOF structures. Furthermore, the computational steps of the suggested control approach are explained. Numerical examples in Section 4 illustrate the robustness of the proposed method in optimizing LQR control approach. Finally, concluding remarks are given in Section 5.

2. LQR control method

The equation of motion for a seismically excited shear-type building with n degrees of freedom controlled by r active actuators can be written as follows

$$\mathbf{M}\ddot{\mathbf{X}}(t)+\mathbf{C}\dot{\mathbf{X}}(t)+\mathbf{K}\mathbf{X}(t)=\mathbf{\Gamma}\mathbf{U}(t)-\mathbf{M}\boldsymbol{\delta}\ddot{x}_g(t) \tag{1}$$

Here, $\mathbf{X}(t)$ is the $(n\times 1)$ relative displacement vector, and $\mathbf{U}(t)$ denotes the $(r\times 1)$ control force vector. $\mathbf{M}$, $\mathbf{C}$ and $\mathbf{K}$, respectively, represent the $(n\times n)$ mass, damping and stiffness matrices. $\ddot{x}_g(t)$ is the one-dimensional ground acceleration of the earthquake. In this equation, $\mathbf{\Gamma}$ and $\boldsymbol{\delta}$ are the $(n\times r)$ location matrix of r controllers and the $(n\times 1)$ location vector of the excitation, respectively. The equation of motion can be rewritten in a form of first-order state-space system

$$\dot{\mathbf{Z}}(t)=\mathbf{A}\mathbf{Z}(t)+\mathbf{B}\mathbf{U}(t)+\mathbf{D}\ddot{x}_g(t) \tag{2}$$

where, $\mathbf{Z}(t)=\{\mathbf{X}(t)\quad \dot{\mathbf{X}}(t)\}^T$ is the $(2n\times 1)$ state vector. The matrices and vectors given in Eq. (2) are as follows

$$\mathbf{A}=\begin{bmatrix}\mathbf{0} & \mathbf{I}\\ -\mathbf{M}^{-1}\mathbf{K} & -\mathbf{M}^{-1}\mathbf{C}\end{bmatrix},\quad \mathbf{B}=\begin{bmatrix}\mathbf{0}\\ \mathbf{M}^{-1}\mathbf{\Gamma}\end{bmatrix},\quad \mathbf{D}=\begin{Bmatrix}\mathbf{0}\\ -\boldsymbol{\delta}\end{Bmatrix} \tag{3}$$

In the procedure of LQR algorithm, a quadratic performance measure is defined

$$J=\frac{1}{2}\int_0^{t_f}\left(\mathbf{Z}^T\,\mathbf{Q}\,\mathbf{Z}+\mathbf{U}^T\,\mathbf{R}\,\mathbf{U}+2\mathbf{Z}^T\,\mathbf{N}\,\mathbf{U}\right)dt \tag{4}$$

In this equation, t_f represents a duration longer than that of the external excitation. $\mathbf{Q}$, $\mathbf{R}$ and $\mathbf{N}$ are weighting matrices regulating the relationship between structural responses and control forces. Another parameter which can be of interest to researchers is the decrease in the absolute acceleration vector ($\ddot{\mathbf{X}}+\boldsymbol{\delta}\ddot{x}_g$). This issue is implicitly considered in Eq. (4), since the equation of motion (1), which should be satisfied throughout the procedure, keeps the relationship between the absolute acceleration and the parameters $\mathbf{X}$, $\dot{\mathbf{X}}$ and $\mathbf{U}$.

The weighting matrices $\mathbf{Q}$ and $\mathbf{R}$ are semi-positive definite and positive definite, respectively. The optimal control force can be obtained by minimizing J under the constraint (2) in the following closed-loop control form

$$\mathbf{U}(t) = \mathbf{G}(t)\,\mathbf{Z}(t) \tag{5}$$

where, the control gain matrix $\mathbf{G}(t)$ is

$$\mathbf{G}(t) = -\mathbf{R}^{-1}\left(\mathbf{B}^T\,\mathbf{P}(t) + \mathbf{N}^T\right) \tag{6}$$

Here, since the external excitation is treated as a white noise (Aldemir *et al.* 2001, Aldemir 2009, Aldemir *et al.* 2012, Fu and Johnson 2017), the term $\ddot{x}_g(t)$ is not considered in the determination of $\mathbf{U}(t)$. The matrix $\mathbf{P}(t)$ is the solution of the matrix Riccati differential equation

$$\dot{\mathbf{P}} + \mathbf{A}^T\,\mathbf{P} + \mathbf{P}\,\mathbf{A} - \left(\mathbf{P}\,\mathbf{B} + \mathbf{N}\right)\mathbf{R}^{-1}\left(\mathbf{B}^T\,\mathbf{P} + \mathbf{N}^T\right) + \mathbf{Q} = \mathbf{0}, \quad \mathbf{P}(t_f) = \mathbf{0} \tag{7}$$

This nonlinear matrix differential equation can be solved by numerical methods (Davison and Maki 1973, Choi 1990, Assimakis *et al*. 1997). Note that the magnitude of t_f is not known in advance for seismic excitations. Moreover, it can be proven that the Riccati matrix $\mathbf{P}(t)$ is almost constant in practical structural control (de Souza 2006, Nguyen and Bestle 2007, Cheng *et al*. 2010, Aldemir *et al.* 2012). Consequently, the matrix differential Eq. (7) changes into an algebraic Riccati equation

$$\mathbf{A}^T\,\mathbf{P} + \mathbf{P}\,\mathbf{A} - \left(\mathbf{P}\,\mathbf{B} + \mathbf{N}\right)\mathbf{R}^{-1}\left(\mathbf{B}^T\,\mathbf{P} + \mathbf{N}^T\right) + \mathbf{Q} = \mathbf{0} \tag{8}$$

Once the weighting matrices $\mathbf{Q}$, $\mathbf{R}$ and $\mathbf{N}$ are assigned based on the structural characteristics, the Riccati matrix $\mathbf{P}$ can be determined through a numerical solution of Eq. (8) (Xu *et al.* 2002, Barbosa and Battista 2007), and subsequently, the constant control gain matrix $\mathbf{G}$ is achieved.

3. Proposed method

Finding the optimal weighting matrices in LQR control method has been of interest to researchers. In this way, several types of weighting matrices are proposed and investigated in the literature (Wong and Yang 2001, Bahar *et al.* 2003, Alavinasab *et al.* 2006). In this paper, the following forms for the matrices $\mathbf{Q}$, $\mathbf{R}$ and $\mathbf{N}$ are chosen

$$\mathbf{Q} = \begin{bmatrix} \mathbf{K} & \mathbf{0} \\ \mathbf{0} & \mathbf{M} \end{bmatrix}, \quad \mathbf{R} = 10^{-\rho}\,\mathbf{\Gamma}^T\,\mathbf{K}^{-1}\,\mathbf{\Gamma}, \quad \mathbf{N} = \mathbf{0} \tag{9}$$

Here, ρ is the regulating parameter adjusting the relationship between the structural responses and active control forces. By applying the matrices given in Eq. (9), the quadratic performance measure J displays a type of total energy. According to Eqs. (5), (6) and (9), the uncontrolled structural responses is obtained when $\rho \to -\infty$. Conversely, great control forces are required when the parameter ρ is increased.

In practical active control systems, the capacity of actuators is limited. Depending on the characteristics of applied actuators, the maximum control forces may be varied and equal to a fraction of the total structural weight

$$u_{\max,j} = \alpha_j\left(\sum_{i=1}^{n} m_i\right) g, \quad j = 1,\ldots,r \tag{10}$$

where, $u_{\max,j}$ and α_j are the maximum force level of the j th actuator and its ratio to the total weight, respectively. m_i represents the mass of the i th story, and g is the gravitational acceleration. When the capacity ratios (α_j for $j = 1,\ldots,r$) are set to zero, the uncontrolled structural responses are achieved. During seismic excitations, the magnitude of required control forces may exceed the capacity of actuators. In this state, the active control force would remain constant at the maximum level (Miller *et al*. 1988, Min *et al.* 2003, Hashemi *et al.* 2016). Accordingly, the control force of actuators is determined as follows

$$u_j(t) = \begin{cases} \operatorname{sgn}(u_{R,j})\,u_{\max,j} & \text{if} \quad \left|u_{R,j}(t)\right| > u_{\max,j} \\ u_{R,j}(t) & \text{if} \quad \left|u_{R,j}(t)\right| \le u_{\max,j} \end{cases}, \quad j = 1,\ldots,r \tag{11}$$

In this equation, $u_{R,j}(t)$ is the required control force for the j th actuator. It is noteworthy that the closed-loop control systems are quite stable in comparison with other systems (Anderson and Moore 1989), and as will be explained in the following subsections, nonlinearities such as Eq. (11) make no impression on the stability of the suggested method.

The objective of this paper is to propose an appropriate approach to improve the efficiency of LQR method for actively controlled structures under seismic excitations. In the following, an estimation of optimal regulating parameter is introduced for SDOF structures. Then, the proposed method is generalized for MDOF structures including one or more active actuators.

3.1 LQR adjustment for SDOF structures

In this subsection, the behavior of SDOF controlled systems subjected to earthquake excitations is investigated. For this purpose, 395 SDOF structures with various natural periods (T) and damping ratios (ξ) are analyzed. Here, the relationship between natural period and frequency is defined as $T = 2\pi/\omega$. The values of T and ξ are, respectively, chosen from the ranges of $0.1\,\text{s} \le T \le 4.0\,\text{s}$ and $0.01 \le \xi \le 0.09$ on a regular basis. In addition, each structure is equipped with an active actuator. The magnitude of the capacity ratio α is assumed to be varied from 0.0 (uncontrolled) to 0.1 (which means $u_{\max} = 0.1\,m\,g$).

In this paper, since the failure of structural elements (such as columns and shear-walls) is caused by the relative displacement, the performance evaluation index J_1 is chosen as the ratio of the maximum controlled displacement to the uncontrolled one

$$J_1 = \underset{\substack{\text{eight} \\ \text{earthquakes}}}{\text{Mean}} \left\{ \frac{\left|x_{\max,C}\right|}{\left|x_{\max,UC}\right|} \right\} \tag{12}$$

Table 1 The list of recorded ground motions used in the analysis of SDOF controlled systems

Name	Date	Station	Type	PGA (g)	f_{m} (Hz)
El Centro	05/19/1940	Imperial Valley Irrigation District (NS)	Far-field	0.348	1.46
Hachinohe	05/16/1968	Hachinohe City (NS)	Far-field	0.229	0.37
Kobe	01/16/1995	Kobe Japanese Meteorological Agency (NS)	Near-field	0.834	2.91
Loma Prieta	10/18/1989	Corralitos (EW)	Near-field	0.483	1.34
Northridge	01/17/1994	Sylmar County Hospital Parking Lot (NS)	Near-field	0.843	0.64
Parkfield	06/28/1966	Temblor (N65E)	Near-field	0.357	2.63
San Fernando	02/09/1971	Pacoima Dam (N76W)	Near-field	1.238	2.33
Taft	07/21/1952	Taft Lincoln School (N21E)	Far-field	0.159	1.36

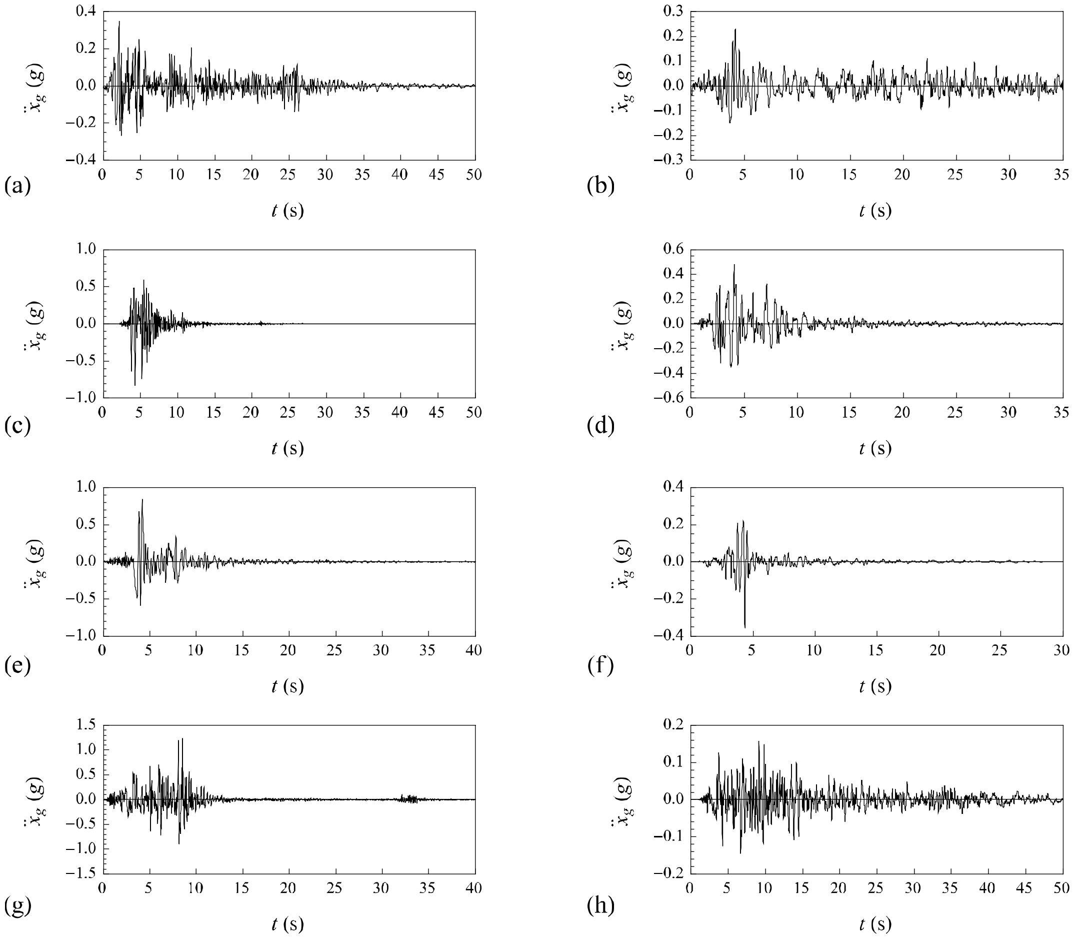

Fig. 1 Time history of ground acceleration for (a) El Centro, (b) Hachinohe, (c) Kobe, (d) Loma Prieta, (e) Northridge, (f) Parkfield, (g) San Fernando and (h) Taft earthquakes

where, the subscripts C and UC denote controlled and uncontrolled cases, respectively. Each SDOF system is separately excited by eight ground motions listed on Table 1. In order to investigate the behavior of structures under different types of earthquakes, both near- and far-field ground motions including a wide range of PGA (peak ground acceleration) are chosen. In addition, the earthquake records (ground acceleration) are illustrated in Fig. 1. The main frequency (f_{m}) of earthquakes, which is obtained from the Fourier transform of the corresponding accelerogram, is given in Table 1.

To obtain the optimal regulating parameter for a SDOF controlled system with specific T, ξ and α, a trial and error procedure is applied. For this purpose, twenty-one values of the regulating parameter ρ are chosen from the range of $-4.0 \le \rho \le 6.0$ on a regular basis, the algebraic Riccati Eq. (8) is solved, and the performance evaluation index J_1 is calculated, separately.

The optimal regulating parameter ρ_{opt} for the supposed controlled system is the one giving the minimum value of performance evaluation index denoted by $J_{1\,\mathrm{min}}$.

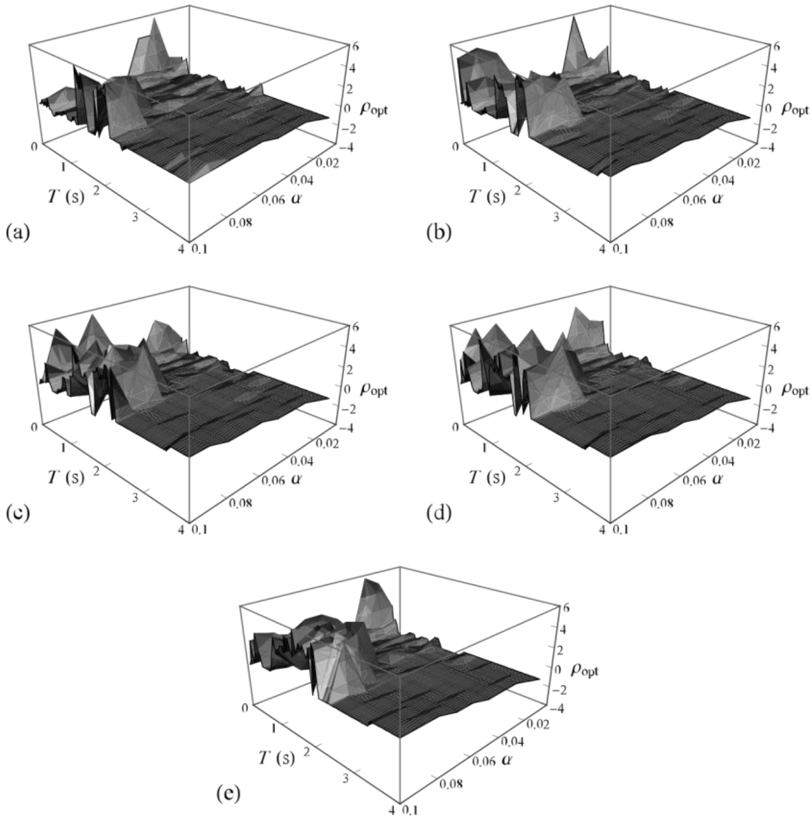

Fig. 2 Optimal regulating parameter for SDOF controlled structures with (a) 0.01, (b) 0.03, (c) 0.05, (d) 0.07 and (e) 0.09 damping ratios

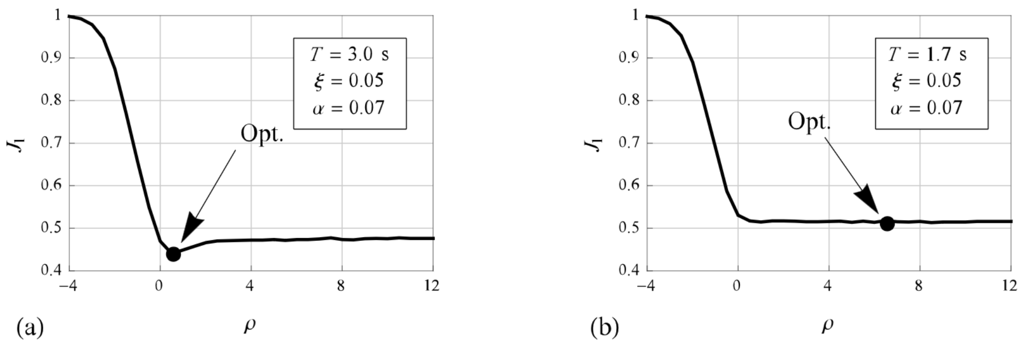

Fig. 3 Relationship between the regulating parameter and the performance evaluation index for (a) smooth and (b) perturbed parts

For all SDOF systems, which their specifications were described previously, this procedure has been done (including 729,960 analyses) without any instability issue. In this way, the fourth order Runge-Kutta method with a constant time step size $\Delta t = 0.005\,\mathrm{s}$ is used. Fig. 2 shows the value of ρ_{opt} relative to the parameters T and α for five different ξ.

As it can be seen, ρ_{opt} surfaces are smooth in most parts, while some perturbations are observed especially in short period structures with higher values of α. As previously explained, the magnitude of ρ_{opt} is obtained from a trial and error procedure resulting the minimum value of performance evaluation index. The authors' experience, which is derived from the investigation of

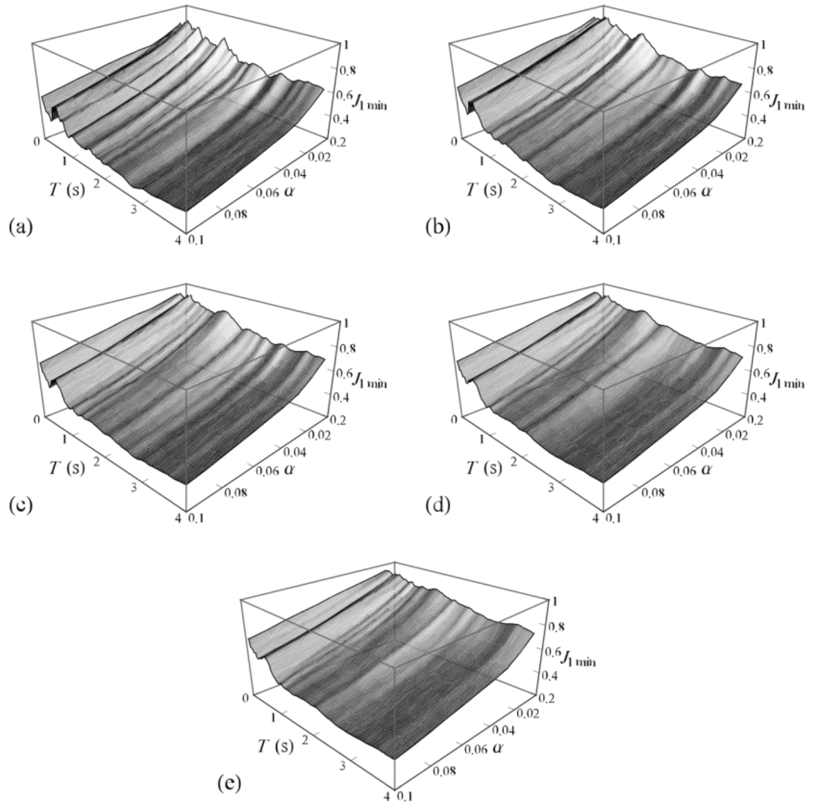

Fig. 4 Minimum performance evaluation index for SDOF controlled structures with (a) 0.01, (b) 0.03, (c) 0.05, (d) 0.07 and (e) 0.09 damping ratios

structural responses, shows that two types of diagrams can describe the relationship between ρ and J_1. The former, which is typically observed in the smooth part, draws an obvious optimum value for ρ, while in the latter type, there is no distinct optimum value. Fig. 3 shows examples of both mentioned types.

In Fig. 3(a), the optimal regulating parameter corresponding to the minimum performance evaluation index can be easily recognized; conversely, the diagram in Fig. 3(b) shows a flat minimum region for a wide range of ρ. In this state, if the structural properties (such as T, ξ and α) slightly change, a large variation in ρ_{opt} can be observed. This would lead to perturbations in some parts of ρ_{opt} surfaces. On the other hand, by considering the existence of the described flat region in perturbed parts, the value of $J_{1\,\min}$ is *not* sensitive to ρ_{opt}. Consequently, variations in $J_{1\,\min}$ are not significant in the vicinity of perturbed parts. Fig. 4 illustrates the minimum performance evaluation index relative to the parameters T and α for five different ξ. As expected, smooth surfaces are obtained for $J_{1\,\min}$. Additionally, by increasing the natural period and capacity ratio, a reduction in the magnitude of $J_{1\,\min}$ can be seen.

As it was previously explained, the perturbation in the value of ρ_{opt} has no considerable effect on $J_{1\,\min}$. Accordingly, the authors propose an estimation of optimum ρ by applying an ordinary least squares regression. In this way, a linear form for the estimated regulating parameter is assumed ($\rho_{\text{est}}(T,\xi,\alpha) = A_0 + A_T\, T + A_\xi\, \xi + A_\alpha\, \alpha$). Then, the constants A_i are calculated by minimizing the distance between ρ_{opt} and ρ_{est} ($\text{Min} \sum_k (\rho_{\text{opt}\,k} - \rho_{\text{est}\,k})^2$):

$$\rho_{\text{est}}(T,\xi,\alpha) = -1.32459 + 0.0504187\,T + 5.35127\,\xi + 27.4614\,\alpha \tag{13}$$

This equation shows the relationship between the estimated regulating parameter and system characteristics. Using ρ_{est} obtained from Eq. (13) for SDOF controlled systems which is formerly described, can cause an error in the calculation of $J_{1\,\min}$. Table 2 provides an error analysis of ρ_{est} and the corresponding minimum performance evaluation index $J_{1\,\text{est}}$. As it is observed, the maximum deviation and standard error between $J_{1\,\text{est}}$ and $J_{1\,\min}$ are, respectively, equal to 0.03 and 0.000097, while these values are substantially greater when ρ_{est} and are compared.

Table 2 Error analysis of estimated regulating parameter and evaluation performance index

Parameter	Maximum deviation	Standard deviation	Standard error
$\rho_{\text{opt}} - \rho_{\text{est}}$	6.44	0.9561	0.015212
$J_{1\,\min} - J_{1\,\text{est}}$	0.03	0.0061	0.000097

This error analysis denotes the efficiency of the proposed estimation for the structural response of SDOF controlled systems.

3.2 Modal formulation for MDOF controlled structures

Transforming the equation of motion into a modal space can be advantageous to have a better understanding of structural behavior, especially in MDOF controlled systems (Wang *et al.* 1999, Cao and Li 2004, Lee *et al.* 2004, Park and Ok 2015). In the previous subsection, the authors present an estimation of the regulating parameter. This estimation is proposed for SDOF structures. In the following, a new modal formulation is introduced to use the suggested ρ_{est} for MDOF controlled structures. For this purpose, the displacement vector is expressed as a linear combination of the first p modes

$$\mathbf{X}(t) = \sum_{k=1}^{p} \boldsymbol{\varphi}_k \, q_k(t) \tag{14}$$

Here, $q_k(t)$ and $\boldsymbol{\varphi}_k$ represent the k th modal coordinate and mode shape, respectively. The mode shape vectors can be normalized through Eq. (15)

$$\left\| \boldsymbol{\delta} - \sum_{k=1}^{p} \boldsymbol{\varphi}_k \right\| = \min \tag{15}$$

In this equation, $\|.\|$ denotes the magnitude of the supposed vector, and $\boldsymbol{\delta}$ is the location vector of the excitation. If all modes of a MDOF structure are considered (the number of applied modes is equal to the number of DOF $p = n$), Eq. (15) becomes

$$\sum_{k=1}^{n} \boldsymbol{\varphi}_k = \boldsymbol{\delta} \tag{16}$$

By considering Eqs. (14) and (16), the equation of motion (1) can be rewritten in the modal space

$$\begin{aligned} & m_k^* \, \ddot{q}_k(t) + c_k^* \, \dot{q}_k(t) + k_k^* \, q_k(t) = \\ & \sum_{j=1}^{r} \Gamma_{jk}^* \, u_j(t) - m_k^* \, \ddot{x}_g(t), \quad k = 1,\ldots,p \end{aligned} \tag{17}$$

where

$$\begin{gathered} m_k^* = \boldsymbol{\varphi}_k^T \, \mathbf{M} \, \boldsymbol{\varphi}_k, \quad c_k^* = \boldsymbol{\varphi}_k^T \, \mathbf{C} \, \boldsymbol{\varphi}_k, \quad k_k^* = \boldsymbol{\varphi}_k^T \, \mathbf{K} \, \boldsymbol{\varphi}_k, \\ k = 1,\ldots,p \end{gathered} \tag{18}$$

$$\Gamma_{jk}^* = \boldsymbol{\varphi}_k^T \, \boldsymbol{\Gamma}_j \quad , \quad j = 1,\ldots,r \quad , \quad k = 1,\ldots,p \tag{19}$$

The vector $\boldsymbol{\Gamma}_j$ is the j th column of the controllers' location matrix $\boldsymbol{\Gamma}$. For each modal coordinate, the authors suggest a separate quadratic performance measure which is similar to Eq. (4)

$$\begin{gathered} J_k^* = \frac{1}{2}\int_0^{t_f} \left(\mathbf{y}_k^T \, \mathbf{Q}_k^* \, \mathbf{y}_k + \mathbf{U}^T \, \mathbf{R}_k^* \, \mathbf{U} + 2\mathbf{y}_k^T \, \mathbf{N}_k^* \, \mathbf{U} \right) dt, \\ k = 1,\ldots,p \end{gathered} \tag{20}$$

Here, $\mathbf{y}_k = \{q_k \quad \dot{q}_k\}^T$. In order to benefit from the outcome of Subsection 3.1, which is corresponding to SDOF controlled structures, the weighting matrices given in Eq. (20) are chosen as follows

$$\begin{gathered} \mathbf{Q}_k^* = \begin{bmatrix} k_k^* & 0 \\ 0 & m_k^* \end{bmatrix}, \\ \mathbf{R}_k^* = \operatorname{diag}\left(10^{-\rho_{1k}} \, {\Gamma_{1k}^*}^2 / k_k^*, \ldots, 10^{-\rho_{rk}} \, {\Gamma_{rk}^*}^2 / k_k^* \right), \\ \mathbf{N}_k^* = \mathbf{0}, \\ k = 1,\ldots,p \end{gathered} \tag{21}$$

Furthermore, the optimum value of the regulating parameters in $\mathbf{R}_k^*$ can be estimated through Eq. (13)

$$\begin{gathered} \rho_{jk} = \rho_{\text{est}}\left(T_k, \xi_k, \alpha_j \left|\Gamma_{jk}^*\right| \sum_{i=1}^{n} m_i \Big/ m_k^* \right), \\ j = 1,\ldots,r, \quad k = 1,\ldots,p \end{gathered} \tag{22}$$

In this equation, T_k and ξ_k are, respectively, the k th modal natural period and damping ratio.

Eq. (20) illustrates the quadratic performance measure for each mode, separately. The summation of all J_k^* gives the performance measure for MDOF controlled systems in the modal space

$$J^* = \sum_{k=1}^{p} J_k^* = \frac{1}{2}\int_0^{t_f} \left(\mathbf{Y}^T \, \mathbf{Q}^* \, \mathbf{Y} + \mathbf{U}^T \, \mathbf{R}^* \, \mathbf{U} \right) dt \tag{23}$$

where, $\mathbf{Y}(t) = \{\mathbf{q}(t) \quad \dot{\mathbf{q}}(t)\}^T$, and the modal weighting matrices are

$$\mathbf{Q}^* = \begin{bmatrix} \mathbf{K}^* & \mathbf{0} \\ \mathbf{0} & \mathbf{M}^* \end{bmatrix} \quad , \quad \mathbf{R}^* = \sum_{k=1}^{p} \mathbf{R}_k^* \tag{24}$$

Here, $\mathbf{q}(t)$ is the vector of modal coordinate. Moreover, $\mathbf{K}^*$ and $\mathbf{M}^*$ represent the modal stiffness and mass matrices, respectively. By using the LQR algorithm, the optimal control force is obtained

$$\mathbf{U}(t) = \mathbf{G}^* \, \mathbf{Y}(t) \tag{25}$$

The calculation process of the modal control gain matrix $\mathbf{G}^*$ is similar to the procedure explained in Section 2. As it is previously mentioned, the magnitude of control forces cannot exceed the capacity of applied actuators described in

Eqs. (10) and (11). In addition, it can be concluded that the stability of SDOF control systems (discussed in the previous subsection) is sufficient to guarantee the stability of the suggested method for MDOF problems.

3.3. Computational steps of proposed control technique

The suggested method is formulized based on a closed-loop control scheme. Consequently, the calculation of the optimum control gain matrix is the main part of the control design procedure. It is worth mentioning that the international system of units (SI) should be used along the calculation. The following computational steps are proposed to obtain the optimum control gain matrix used in the suggested algorithm:

1- Computation of the first p natural periods T_k and mode shapes $\boldsymbol{\varphi}_k$ of the structure: Based on the number of sensors and the intended level of accuracy of the problem, the value of p is chosen. To obtain T_k and $\boldsymbol{\varphi}_k$, standard numerical methods (e.g., Rayleigh quotient iteration, Lanczos algorithm or inverse power method) can be applied.

2- Calculation of modal structural characteristics m_k^*, c_k^*, k_k^* and Γ_{jk}^* from Eqs. (18) and (19).

3- Estimating the optimum value of regulating parameters ρ_{jk} for each mode by considering Eqs. (13) and (22).

4- Determination of weighting matrices $\mathbf{Q}_k^*$ and $\mathbf{R}_k^*$ for each mode from Eq. (21).

5- Obtaining modal weighting matrices $\mathbf{Q}^*$ and $\mathbf{R}^*$ from Eq. (24).

6- Transforming the modal equation of motion into a form of first-order state-space system: Similar to the procedure described in Section 2, the vectors and matrices $\mathbf{A}^*$, $\mathbf{B}^*$ and $\mathbf{D}^*$ can be obtained.

7- Solution of algebraic Riccati Eq. (8) by considering $\mathbf{N}^* = \mathbf{0}$.

8- Calculation of modal control gain matrix $\mathbf{G}^*$ according to Eq. (6).

Finally, when the structure is subjected to earthquake excitations, the optimal control force can be computed by using Eq. (25).

4. Numerical examples

In order to illustrate the performance of the proposed control method, five seismically excited shear-type buildings equipped with active control devices are investigated. These buildings were previously studied by researchers (Soong 1988, Schmitendorf *et al.* 1994, Singh *et al.* 1997, Lu *et al.* 1998, Min *et al.* 2003, Alavinasab *et al.* 2006, Park and Ok 2015). In this section, the structural responses obtained by the suggested method are compared with the results of other control techniques for the same seismic excitations given by the mentioned references. This comparison shows the robustness of the authors' method. Note that all modes are considered to have a better analogy, although the proposed technique is capable of using fewer mode shapes. As it is previously mentioned, the international system of units (SI) is used along the control design procedure. Fig. 5 demonstrates the schematics of the supposed buildings. As it can be seen, all examples are MDOF structures with one or more active actuators. Here, the applied control devices are active mass damper, active tendons and active bracing. To have a better understanding of structural behavior, graphical representations and tabulated data with additional information are provided.

4.1 Ten-story building with AMD placed on the rooftop

Fig. 5(a) illustrates a ten-story shear-type building equipped with one active mass damper (AMD) on the rooftop (Min *et al.* 2003). The mass of each floor is 50 ton, and the stiffness of each story is $k_i = 1.5\times10^4$ kN/m for $i = 1,\ldots,4$, $k_i = 1.05\times10^4$ kN/m for $i = 5,6,7$ and $k_i = 7.35\times10^3$ kN/m for $i = 8,9,10$. The value of damping ratio for all modes is assumed to be $\xi = 0.02$. The maximum control force that AMD can provide is $u_{\max} = 84.16$ kN. The weighting matrices $\mathbf{Q}^*$ and $\mathbf{R}^*$ can be estimated by the proposed method as follows

$$\begin{aligned}\mathbf{Q}^* = \mathrm{diag}\big(&2.269\times10^6, 2.422\times10^6, 2.198\times10^6,\\ &1.452\times10^6, 1.894\times10^6, 1.264\times10^6,\\ &7.591\times10^5, 8.740\times10^5, 1.291\times10^6,\\ &5.771\times10^5, 3.996\times10^5, 5.958\times10^4,\\ &2.029\times10^4, 6.871\times10^3, 5.936\times10^3,\\ &2.872\times10^3, 1.445\times10^3, 1.267\times10^3,\\ &1.577\times10^3, 5.327\times10^2\big),\\ \mathbf{R}^* = \big[&1.575\times10^{-6}\big]\end{aligned} \tag{26}$$

The building is subjected to the ground acceleration of El Centro earthquake (1940, Imperial Valley Irrigation District NS) in both controlled and uncontrolled cases. The AMD generates the control force based on the proposed control law. In Fig. 6. the relative displacement $x(t)$, relative velocity $\dot{x}(t)$ and absolute acceleration $\ddot{x}_a(t)$ of the top floor are shown. Here, the black curves are corresponding to the controlled structural responses. These carves indicate a considerable reduction in responses. The ratios of maximum controlled responses to the uncontrolled ones are 0.48, 0.60 and 0.74 for $x(t)$, $\dot{x}(t)$ and $\ddot{x}_a(t)$, respectively, while the control technique which is provided in (Min *et al.* 2003) obtains greater values (0.51 for the relative displacement and 0.79 for the absolute acceleration of the top floor). This comparison demonstrates the superiority of the suggested method.

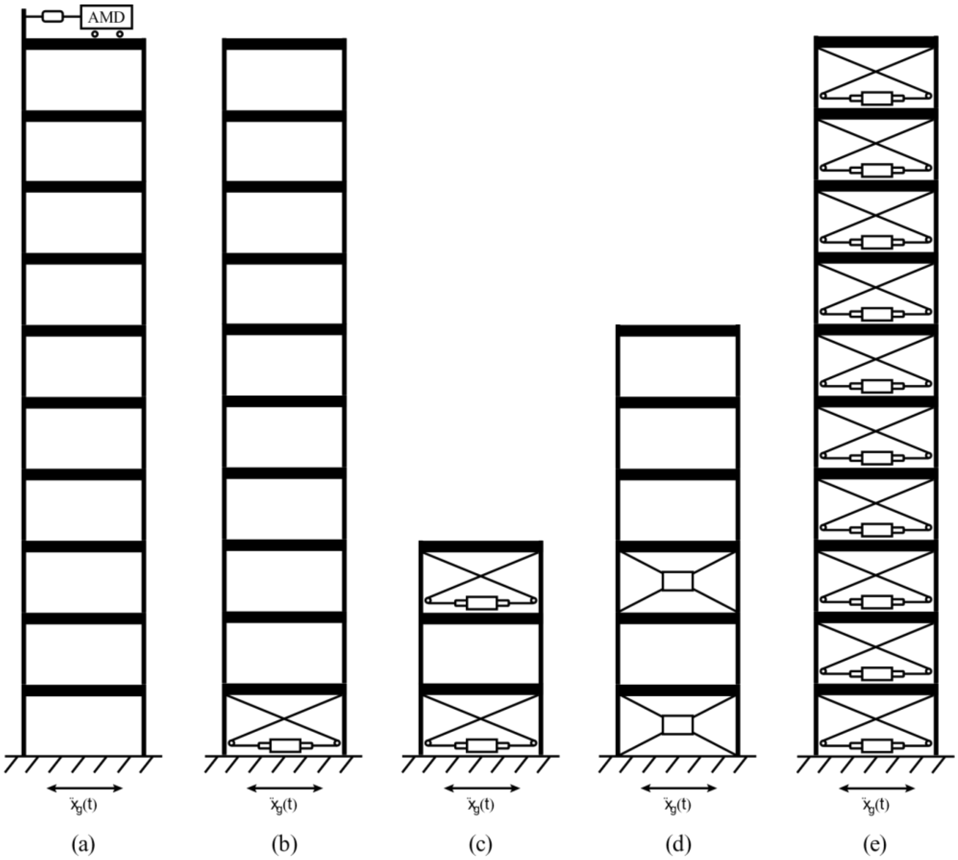

Fig. 5 Schematics of shear-type buildings investigated in numerical examples

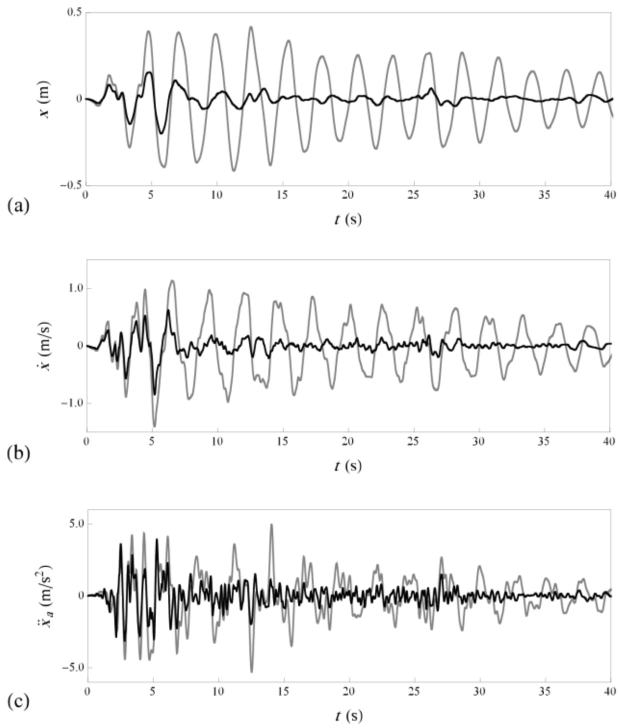

Fig. 6 Time history of top floor (a) relative displacement, (b) relative velocity and (c) absolute acceleration

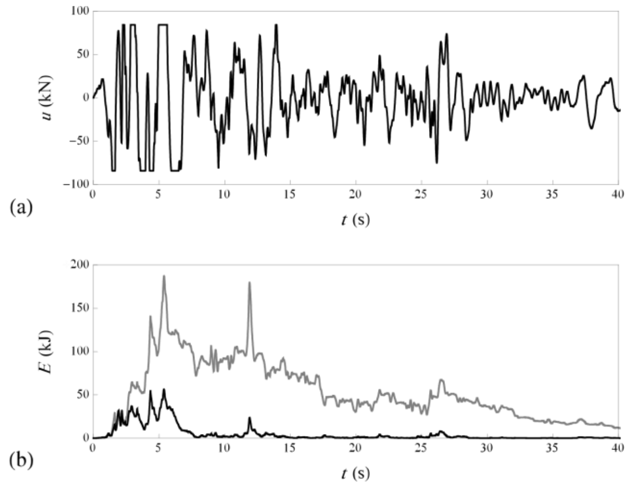

Fig. 7 Time history of (a) control force and (b) structural energy

The control force and structural energy are displayed in Fig. 7. As it is observed, the magnitude of the generated control force remains constant when the required control force $u_R(t)$, which is calculated by the LQR method, is greater than the maximum level $u_{\max}$

The structural energy $E(t)$ consists of potential energy and kinetic energy (Wong and Yang 2001, Alavinasab *et al.* 2006)

$$E(t) = \mathbf{Z}(t)^T \mathbf{Q} \mathbf{Z}(t) \tag{27}$$

Fig. 7(b) illustrates the structural energy in both controlled (black) and uncontrolled (gray) cases. This figure shows a 69.9% reduction in the maximum value of structural energy.

4.2 Ten-story building with active tendons on the first floor

Here, a ten-story building equipped with active tendons on the first floor is investigated. The schematic of this shear-type building is displayed in Fig. 5(b). Each story has the same structural characteristics ($m_i = 357.24$ ton , $c_i = 6.15\times10^3$ kN.s/m and $k_i = 6.5498\times10^5$ kN/m for $i = 1,\ldots,10$). The controlled and uncontrolled structural responses of the building related to four different seismic excitations were previously studied in (Singh *et al.* 1997). The supposed ground acceleration records are El Centro (1940, Imperial Valley Irrigation District NS), San Fernando (1971, Pacoima Dam N76W), Loma Prieta (1989, Corralitos NS) and Kern County (1952, Hollywood Basement Site NS). In this example, all records are scaled uniformly to a PGA of $0.3g$. The magnitude of $u_{\max}$, which is normalized by a floor weight, is assumed to be 3.52 , 2.39 , 2.65 and 5.36 for the mentioned earthquakes, respectively. These values are chosen from (Singh *et al.* 1997). The suggested method proposes the following weighting matrices $\mathbf{Q}^*$ and $\mathbf{R}^*$

$$\begin{aligned}\mathbf{Q}^* = \operatorname{diag}\big(&1.241\times10^8, 1.186\times10^8, 1.081\times10^8,\\ &9.357\times10^7, 7.626\times10^7, 5.772\times10^7,\\ &3.959\times10^7, 2.349\times10^7, 1.084\times10^7,\\ &2.771\times10^6, 3.029\times10^6, 3.265\times10^5,\\ &1.104\times10^5, 5.103\times10^4, 2.675\times10^4,\\ &1.465\times10^4, 7.908\times10^3, 3.945\times10^3,\\ &1.619\times10^3, 3.865\times10^2\big)\\ \mathbf{R}^* = \big[&2.607\times10^{-11}\big]\end{aligned} \tag{28}$$

The top floor relative displacement $x(t)$, base shear $V_x(t)$ and control force $u(t)$ for the ten-story building subjected to the scaled ground acceleration of El Centro are given in Fig. 8. The structural responses are shown in both controlled (black) and uncontrolled (gray) cases. The proposed control law regulates the control force generated by active tendons. This figure illustrates a notable reduction in the top floor relative displacement and base shear. The comparison between the maximum controlled responses and the uncontrolled ones indicates 65.3% and 61.4% reduction in $x(t)$ and $V_x(t)$, respectively, while these values obtained from the control technique provided in (Singh *et al.* 1997) are 60.0% and 26.2%. Note that the difference in the maximum of base shear is significant.

The proposed control analysis is separately done for the ten-story building under four scaled earthquakes. Maximum relative displacements are calculated and displayed in Fig. 9. The gray curves represent uncontrolled responses, and the maximum displacements obtained by the suggested procedure and the method introduced in (Singh *et al.* 1997) are demonstrated by black solid and black dashed curves, respectively.

As it is observed, the authors' method shows a better performance in the maximum displacement of the rooftop for all earthquake records. Moreover, this superiority can be seen on average for 85.0% of floor levels, especially in

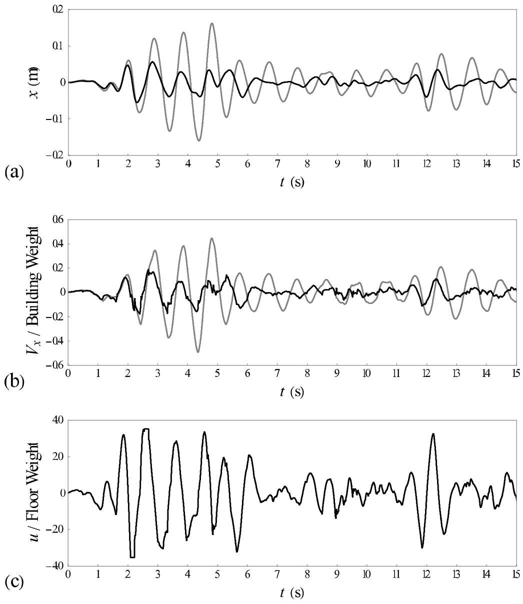

Fig. 8 Time history of (a) top floor relative displacement, (b) base shear and (c) control force

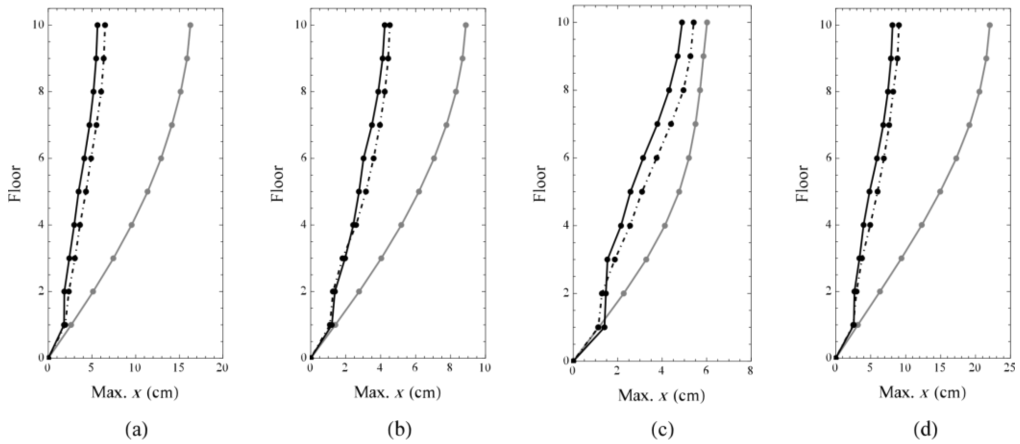

Fig. 9 Maximum relative displacements with respect to (a) El Centro, (b) San Fernando, (c) Loma Prieta and (d) Kern County earthquakes

middle and top stories of the structure. The formation of curves drawn in Fig. 9 is approximately similar (except for Loma Prieta earthquake). In the El Centro case, the proposed method is more efficient and comparable with other records. It is worth mentioning that the maximum displacement of the first floor calculated by the suggested procedure for Loma Prieta earthquake is greater than the uncontrolled state. Conversely, the best performance in the reduction of structural response is observed at middle levels for this record.

The maximum values of interstory displacement and absolute acceleration are shown in Figs. 10 and 11, respectively. As it can be seen, the maximum interstory displacements decrease at all levels when the active control system is used (black curves), while the maximum absolute accelerations corresponding to the levels close to active tendons increase.

4.3 Three-story building with active tendon systems

A three-story shear-type building equipped with two active control systems is shown in Fig. 5(c). The actuators are placed in the first and third stories. This structure was previously studied by researchers (Gluck *et al*. 1996, Alavinasab *et al.* 2006). The mass, damping and stiffness matrices are as follows

$$\mathbf{M}=\begin{bmatrix}200.40 & 0 & 0\\ 0 & 200.40 & 0\\ 0 & 0 & 178.00\end{bmatrix}\text{kg}$$
$$\mathbf{C}=\begin{bmatrix}264.99 & -78.09 & -16.08\\ -78.09 & 246.89 & -92.15\\ -16.08 & -92.15 & 162.02\end{bmatrix}\text{N.s/m} \tag{29}$$
$$\mathbf{K}=\begin{bmatrix}238.932 & -119.466 & 0\\ -119.466 & 238.932 & -119.466\\ 0 & -119.466 & 119.466\end{bmatrix}\text{kN/m}$$

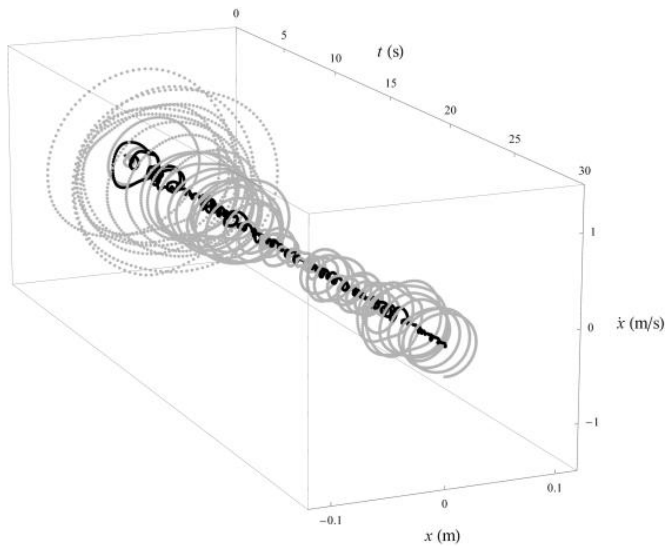

Fig. 12 Time history of top floor relative displacement and velocity

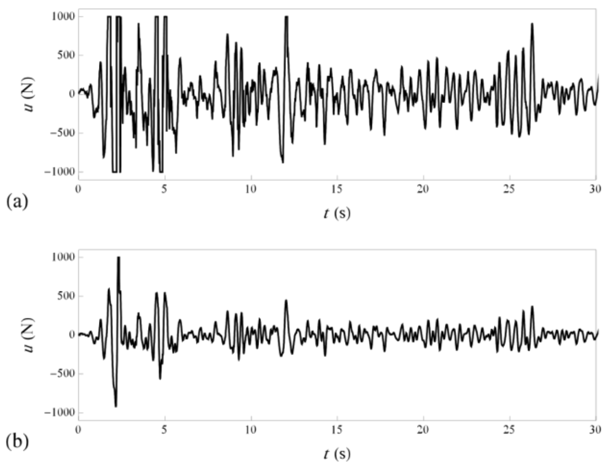

Fig. 13 Time history of active control forces of actuators located on (a) the first and (b) the third floors

The maximum control force that active tendons can provide is $u_{\max,\,j} = 1000\ \text{N}$ for $j = 1, 2$. The weighting matrices $\mathbf{Q}^*$ and $\mathbf{R}^*$ estimated by the proposed method are as follows

$$\mathbf{Q}^* = \text{diag}\Big(6.664\times10^4, 4.102\times10^4, 1.181\times10^4, 5.304\times10^2, 4.242\times10^1, 6.015\times10^0\Big) \quad (30)$$
$$\mathbf{R}^* = \text{diag}\Big(8.210\times10^{-8}, 7.503\times10^{-7}\Big)$$

This building is subjected to three seismic excitations. The supposed ground acceleration records are El Centro (1940, Imperial Valley Irrigation District NS), Hachinohe (1968, Hachinohe City NS) and Taft (1952, Taft Lincoln School S69E). The proposed control law regulates the control force generated by tendons. Fig. 12 illustrates the relative displacement and velocity of the rooftop in both controlled (black) and uncontrolled (gray) cases for the El Centro earthquake. The ratios of maximum controlled displacement and velocity to the uncontrolled ones are 0.29 and 0.27, respectively.

The time history of active control forces is given in Fig. 13, As it is observed, the magnitude of control forces provided by the actuator placed on the first floor on average is greater than the other actuator.

In order to evaluate the performance of the proposed method in the estimation of weighting matrices for MDOF structures with multiple active actuators, the seismic structural responses obtained by the authors' control method is compared with the responses given by an LQR technique which is optimized through a trial and error procedure. To have a better analogy, the LQR method is applied in the modal space. Additionally, the modal weighting matrix $\mathbf{Q}^*$ is chosen from Eq. (30). The matrix $\mathbf{R}^*$ is assumed to be diagonal and its entries are obtained by trial and error. In this way, a *large* number of diagonal entries are chosen to achieve the greatest decrease in the maximum displacement of the rooftop. This procedure is done for each earthquake record, separately

Table 3 Structural responses of the three-story building

Earthquake	Floor	Uncontrolled Max. x (cm)	Uncontrolled Max. Δx (cm)	LQR with trial and error Max. x (cm)	LQR with trial and error Max. Δx (cm)	LQR with trial and error RMS u (N)	Proposed method Max. x (cm)	Proposed method Max. Δx (cm)	Proposed method RMS u (N)
El Centro	1st	4.94	4.94	1.52	1.52	256.3	1.57	1.57	258.7
	2nd	8.91	3.99	3.01	1.68	–	3.06	1.71	–
	3rd	11.1	2.17	3.15	0.81	130.2	3.25	0.79	121.4
Hachinohe	1st	1.92	1.92	0.52	0.52	236.3	0.54	0.54	234.9
	2nd	3.46	1.55	1.02	0.78	–	1.05	0.78	–
	3rd	4.27	0.90	1.18	0.27	93.5	1.23	0.27	90.7
Taft	1st	1.91	1.91	0.43	0.43	156.9	0.44	0.44	156.3
	2nd	3.26	1.35	0.81	0.64	–	0.85	0.65	–
	3rd	3.93	0.78	0.95	0.23	63.9	1.00	0.23	62.7

$$\begin{aligned}
\mathbf{R}^*_{\text{El Centro}} &= \operatorname{diag}\left(1.277\times10^{-7}, 8.439\times10^{-8}\right)\\
\mathbf{R}^*_{\text{Hachinohe}} &= \operatorname{diag}\left(1.299\times10^{-8}, 9.745\times10^{-8}\right)\\
\mathbf{R}^*_{\text{Taft}} &= \operatorname{diag}\left(7.308\times10^{-9}, 1.285\times10^{-7}\right)
\end{aligned} \tag{31}$$

As it is seen, the magnitude of optimum matrix $\mathbf{R}^*$ is varied for each earthquake record.

Table 3 presents the structural responses in uncontrolled, LQR and proposed cases. In this table, the maximum relative displacement, maximum interstory displacement and root mean square (RMS) of control forces are given for all floors. As it is observed, the maximum relative and interstory displacements computed through LQR are *slightly* smaller than the displacements obtained by the suggested control method. This comparison reveals the efficiency of the proposed technique. Note that, since there is no active tendon system on the second floor, the controlled interstory displacements at this level are greater than the other floors for all records. In addition, the RMS of control force generated by active tendons on the first floor is remarkably larger than the other in both controlled cases.

4.4 Six-story building with active bracing systems

The schematic of a six-story building is displayed in Fig. 5(d). This structure is equipped with two active bracing systems, which are installed on the first and third floors. Each story has the same structural properties as follows: $m_i = 345.6$ ton, $c_i = 2.937\times10^3$ kN.s/m and $k_i = 3.404\times10^5$ kN/m for $i = 1,\ldots,6$. The controlled and uncontrolled structural responses of the building corresponding to the ground acceleration of El Centro earthquake (1940, Imperial Valley Irrigation District NS) were previously studied in (Schmitendorf *et al.* 1994, Lu *et al.* 1998).

In order to evaluate the efficiency of the suggested method, the maximum control forces provided by active bracing systems are chosen from (Schmitendorf *et al*. 1994). Here, two cases are investigated. In Case A, the magnitudes of maximum control forces of actuators placed on the first and third floors are $u_{\max,1} = 7706$ kN and $u_{\max,2} = 3035$ kN, respectively. These values are chosen $u_{\max,1} = 1760$ kN and $u_{\max,2} = 1010$ kN in Case B. The proposed weighting matrices $\mathbf{Q}^*$ and $\mathbf{R}^*$ for both cases are as follows

$$\begin{aligned}
\mathbf{Q}^*_{\text{Cases A \& B}} = \operatorname{diag}\big(&1.032\times10^{8}, 9.157\times10^{7}, 7.094\times10^{7},\\
&4.606\times10^{7}, 2.262\times10^{7}, 5.999\times10^{6},\\
&1.803\times10^{6}, 1.848\times10^{5}, 5.580\times10^{4},\\
&2.087\times10^{4}, 7.323\times10^{3}, 1.615\times10^{3}\big)\\
\mathbf{R}^*_{\text{Case A}} = \operatorname{diag}&\left(2.694\times10^{-12}, 5.137\times10^{-10}\right)\\
\mathbf{R}^*_{\text{Case B}} = \operatorname{diag}&\left(1.696\times10^{-9}, 3.197\times10^{-9}\right)
\end{aligned} \tag{32}$$

The controlled and uncontrolled structural responses are obtained for both cases. To have a better comparison between the proposed control procedure and the method given by (Schmitendorf *et al.* 1994), the following performance evaluation indexes are defined and separately calculated for each floor

$$J_2 = \frac{\left|\Delta x_{\max,C}\right|}{\left|\Delta x_{\max,UC}\right|} \tag{33}$$

$$J_3 = \frac{\left|\ddot{x}_{a\,\max,C}\right|}{\left|\ddot{x}_{a\,\max,UC}\right|} \tag{34}$$

where, Δx denotes the interstory displacement, and $\ddot{x}_a$ is the absolute acceleration of the supposed floor. The subscripts C and UC represent controlled and uncontrolled cases, respectively. Table 4 shows the values of indexes J_2 and J_3 obtained by both controlled methods for all floors in Cases A and B. In this example, the structure is subjected to the ground acceleration of El Centro earthquake.

As it is observed, the proposed procedure gives the interstory displacements less than or equal to the values computed by (Schmitendorf *et al*. 1994) in both Cases A and B. Additionally, the magnitudes of J_3 obtained by the authors' method are greater *only* for the two first floors. This issue demonstrates the superiority of the suggested control technique.

Table 4 Performance evaluation indexes calculated for the six-story building

Floor	Case A				Case B			
	Ref. (Schmitendorf *et al*. 1994)		Proposed		Ref. (Schmitendorf *et al*. 1994)		Proposed	
	J_2	J_3	J_2	J_3	J_2	J_3	J_2	J_3
1st	0.37	1.25	0.28	3.48	0.61	0.87	0.58	1.22
2nd	0.59	0.87	0.48	0.90	0.65	0.76	0.62	1.01
3rd	0.63	0.79	0.38	0.49	0.69	0.70	0.59	0.64
4th	0.52	0.62	0.52	0.52	0.71	0.69	0.70	0.64
5th	0.69	0.68	0.56	0.53	0.74	0.73	0.74	0.72
6th	0.69	0.70	0.61	0.61	0.77	0.78	0.77	0.77

4.5 Ten-story building with active tendon systems

In this example, the structural behavior of a ten-story shear-type building equipped with active tendons is investigated. In each story, an active tendon system is installed. This building is shown in Fig. 5(e). The mass of floors is $m_i = 350.0$ ton for $i = 1,2$ and $m_i = 280.0$ ton for $i = 3,\ldots,10$. The story stiffness is $k_i = 506.0\times10^3$ kN/m for $i = 1,2$ and $k_i = 458.7\times10^3$ kN/m for $i = 3,\ldots,10$. The damping matrix is calculated by Rayleigh approach, and the damping ratio for the first and second modes is assumed to be 1.0%.

The structural behavior of the building was previously studied in (Park and Ok 2015) for three scenarios. First, the structural responses under the normal condition are obtained (Case A). In Case B, it is assumed that the active devices in the first, third and eighth stories break down during excitations. For the third scenario (Case C), a perturbation in the stiffness matrix of the structure is considered

$$\mathbf{K}_{SV} = (1+\delta)\mathbf{K}_{NC} \tag{35}$$

where, the subscripts NC and SV denote "Normal Condition" and "Stiffness Variation" cases, respectively. δ is the perturbation ratio and assumed to be -20%.

The building is subjected to two seismic excitations. The ground acceleration records are El Centro (1940, Imperial Valley Irrigation District NS) and Northridge (1994, Sylmar County Hospital Parking Lot NS). For three described scenarios, the maximum control forces which can be provided by active tendons are separately listed in Table 5 for two earthquake records. These values are chosen from (Park and Ok 2015).

The proposed control method and the modal-space reference-model-tracking fuzzy control (MRFC) approach introduced by (Park and Ok 2015) are separately applied for the ten-story building under El Centro and Northridge earthquakes. In the suggested control design procedure, since it is assumed that the structural characteristics remain constant during seismic excitations, the modal gain matrix is calculated once for all scenarios based on the capacity of active actuators under "Normal Condition" (the values given in Case A). In this way, the weighting matrices $\mathbf{Q}^*$ and $\mathbf{R}^*$ are obtained as follows

$$\begin{aligned}
&\mathbf{Q}^*_{\text{El Centro \& Northridge}} = \\
&\mathrm{diag}\big(9.115\times10^{7}, 1.027\times10^{8}, 9.667\times10^{7}, \\
&\quad 6.901\times10^{7}, 5.127\times10^{7}, 4.750\times10^{7}, \\
&\quad 3.447\times10^{7}, 1.082\times10^{7}, 2.125\times10^{6}, \\
&\quad 3.102\times10^{5}, 2.416\times10^{6}, 3.188\times10^{5}, \\
&\quad 1.159\times10^{5}, 4.424\times10^{4}, 2.074\times10^{4}, \\
&\quad 1.384\times10^{4}, 8.051\times10^{3}, 2.129\times10^{3}, \\
&\quad 3.642\times10^{2}, 4.875\times10^{1}\big) \\
&\mathbf{R}^*_{\text{El Centro}} = \\
&\mathrm{diag}\big(1.246\times10^{-9}, 1.281\times10^{-9}, 1.263\times10^{-9}, \\
&\quad 1.361\times10^{-9}, 1.455\times10^{-9}, 1.440\times10^{-9}, \\
&\quad 1.287\times10^{-9}, 9.816\times10^{-10}, 7.210\times10^{-10}, \\
&\quad 7.920\times10^{-10}\big) \\
&\mathbf{R}^*_{\text{Northridge}} = \\
&\mathrm{diag}\big(1.519\times10^{-10}, 1.639\times10^{-10}, 1.250\times10^{-10}, \\
&\quad 1.803\times10^{-10}, 2.844\times10^{-10}, 3.718\times10^{-10}, \\
&\quad 4.175\times10^{-10}, 4.348\times10^{-10}, 3.511\times10^{-10}, \\
&\quad 1.782\times10^{-10}\big)
\end{aligned} \tag{36}$$

Subsequently, the design gain matrix $\mathbf{G}^*$ is calculated prior to applying any seismic excitation. This matrix will remain unchanged for all cases.

On the other hand, in order to have a better analogy, the maximum control forces *along* seismic excitations are chosen from Table 5 for both control methods. Fig. 14 shows the maximum interstory displacements given by the authors' technique (black solid curves), MRFC approach (black dashed curves) and uncontrolled case (gray curves) for the El Centro earthquake. As it can be seen, the proposed method obtains a greater value *only* for the rooftop in the normal condition. In Case B, the maximum interstory displacements increase in the stories that the breakdown of actuators is considered; conversely, the suggested control technique obtains smaller values at other floor levels in comparison with the interstory displacements calculated by the MRFC approach. Both control algorithms give similar structural responses in Case C at most levels.

Table 5 Maximum control forces of actuators placed in the ten-story building (kN)

Floor	El Centro			Northridge		
	Case A: Normal condition	Case B: Breakdown of actuators	Case C: -20% stiffness variation	Case A: Normal condition	Case B: Breakdown of actuators	Case C: -20% stiffness variation
1st	3235.9	–	3192.4	7615.5	–	15398.2
2nd	3151.1	6229.0	3090.9	7542.9	15641.9	15245.4
3rd	3231.5	–	3123.9	7953.7	–	15152.8
4th	2987.0	4906.6	2835.1	7428.4	13349.3	14099.9
5th	2671.8	4087.0	2525.1	6611.9	10835.4	12556.3
6th	2311.4	3301.1	2298.6	6075.7	9313.4	10705.3
7th	1917.6	3063.8	2015.2	5679.8	8159.6	8699.8
8th	1474.3	–	1639.6	4923.9	–	6603.3
9th	985.9	1845.7	1170.0	3667.8	4995.9	4436.1
10th	499.1	965.9	605.4	1959.2	2658.8	2225.4

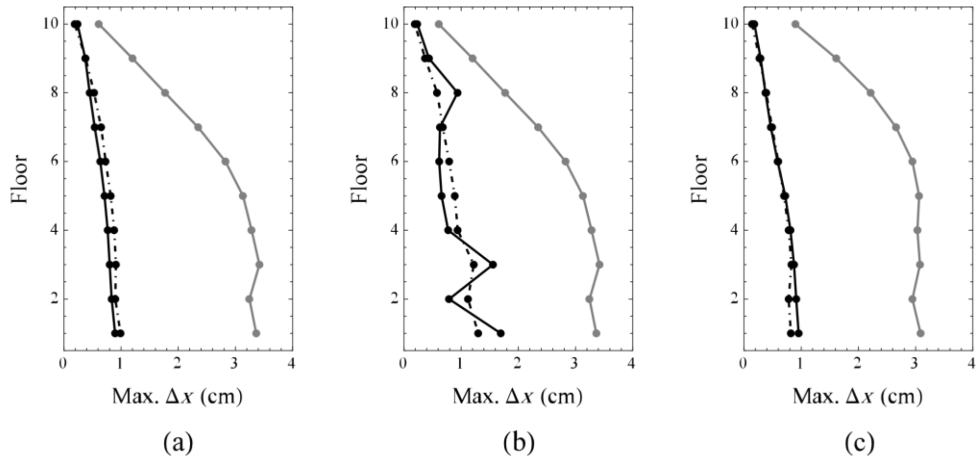

Fig. 14 Maximum interstory displacements with respect to El Centro earthquake in (a) Case A, (b) Case B and (c) Case C

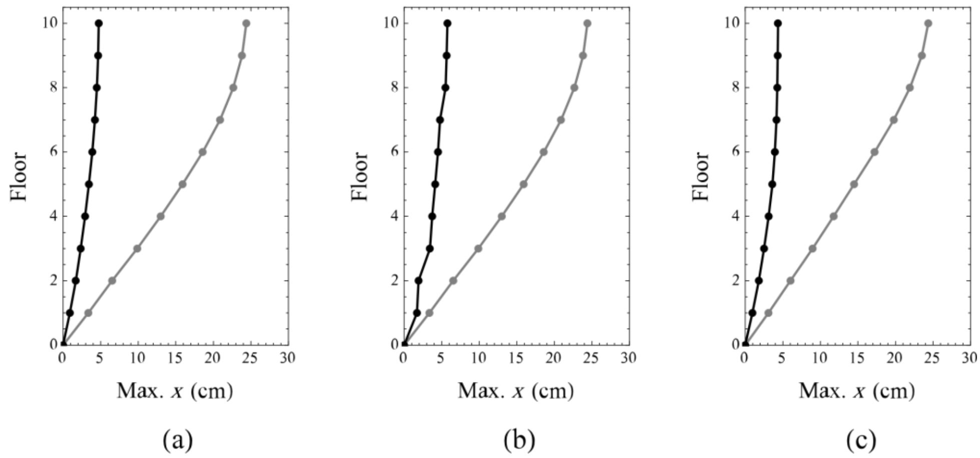

Fig. 15 Maximum relative displacements with respect to El Centro earthquake in (a) Case A, (b) Case B and (c) Case C

The maximum relative displacements are given in Fig. 15 for both controlled (black) and uncontrolled (gray) cases. The decrease in this parameter is significant at higher levels. In addition, the maximum absolute accelerations become almost invariant at all levels (Fig. 16).

Fig. 17 illustrates the maximum interstory displacements for both controlled and uncontrolled cases with respect to the Northridge earthquake. The formation of curves in Case A reveals a better performance of the proposed method in the seismic behavior of the building for all stories. In the case of actuator failures (Case B), the structural responses obtained by the suggested technique is *slightly* greater than the values computed through the MRFC approach at the first, third, fourth and eighth floors.

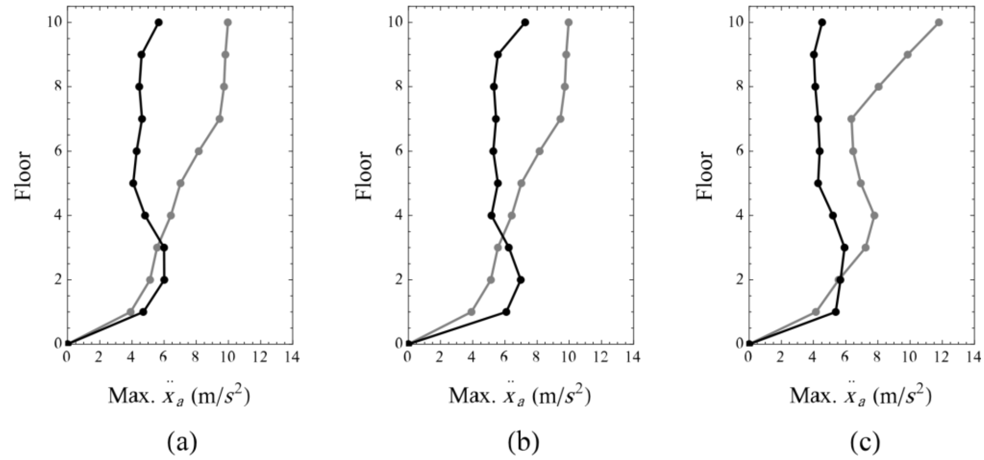

Fig. 16 Maximum absolute accelerations with respect to El Centro earthquake in (a) Case A, (b) Case B and (c) Case C

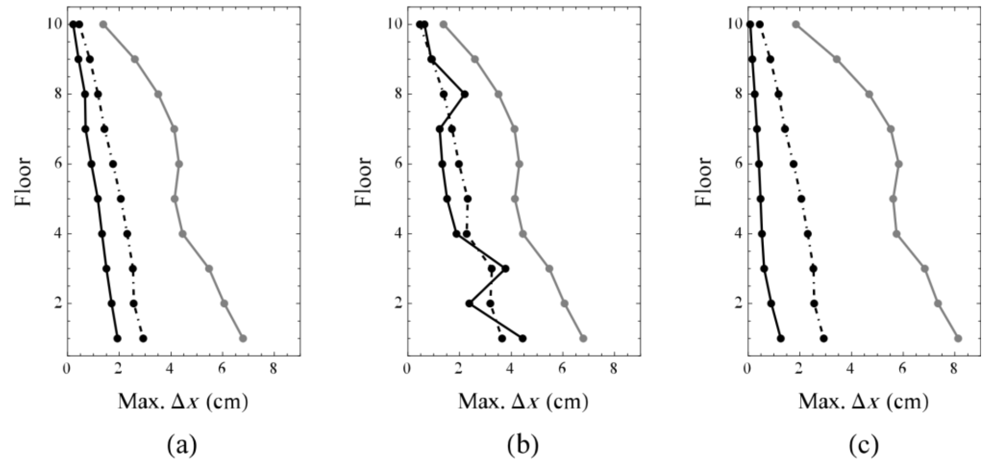

Fig. 17 Maximum interstory displacements with respect to Northridge earthquake in (a) Case A, (b) Case B and (c) Case C

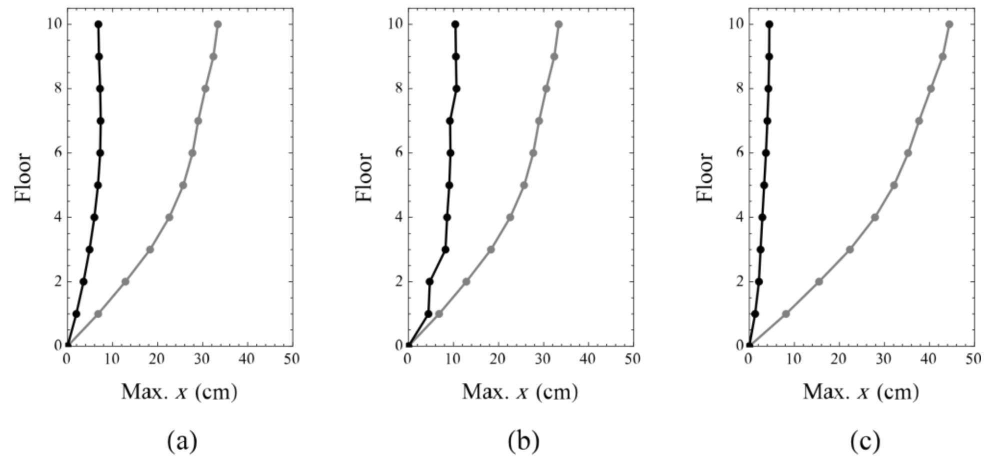

Fig. 18 Maximum relative displacements with respect to Northridge earthquake in (a) Case A, (b) Case B and (c) Case C

A similar phenomenon was observed for the El Centro record. Fig. 17(c) shows a considerable decrease in structural responses given by the authors' control algorithm in the case of –20% stiffness variation. This issue demonstrates that the magnitudes of maximum control forces assumed by (Park and Ok 2015) are excessively large.

Generally, although the suggested control design procedure is done according to "Normal Condition", 71.7% of maximum interstory displacements obtained by

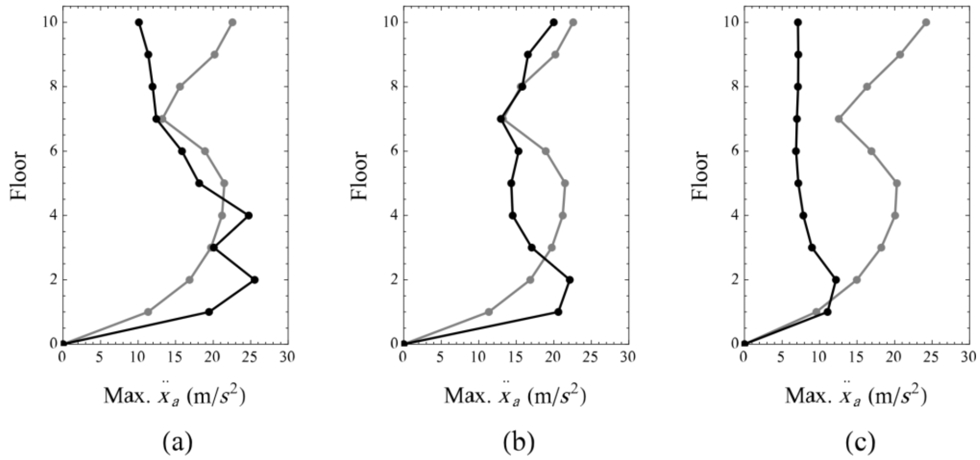

Fig. 19 Maximum absolute accelerations with respect to Northridge earthquake in (a) Case A, (b) Case B and (c) Case C

the proposed method is smaller than the values calculated through the MRFC approach for all scenarios.

Similar to the previous ground motion, a considerable decrease in the maximum relative displacements is observed (Fig. 18), while a particular pattern for the maximum absolute accelerations cannot be derived (Fig. 19).

5. Conclusions

The seismic response of structures can be remarkably reduced through using active control systems adjusted by an LQR algorithm. The weighting matrices in LQR play an important role in keeping a balance between the structural responses and control forces while the building is excited by external forces.

In this paper, a new formulation is introduced to regulate the control LQR approach for seismically excited shear-type buildings equipped with active devices, such as AMD, active tendons and active bracing. For this purpose, first, the seismic behavior of 395 SDOF systems with various natural periods and damping ratios is investigated. In this way, eight earthquake records are used as ground accelerations, and the corresponding maximum relative displacements are obtained in both controlled and uncontrolled cases. The maximum control force provided by the active actuator is assumed to be varied from zero (uncontrolled) to ten percent of the total weight. Here, the LQR method is applied as the control algorithm, and an energy-type quadratic performance measure including a regulating parameter is chosen. Additionally, the performance evaluation index is assumed to be the ratio of the maximum controlled displacement to the uncontrolled one. For each SDOF system with specific structural characteristics and maximum control force, the optimal regulating parameter is calculated through a trial and error procedure. In this state, over 700,000 analyses have been done. The study of results shows smooth changes in the performance evaluation index, although variations in the optimal regulating parameter can be significant. By considering this issue, the authors provide an estimation of optimal regulating parameter for SDOF systems. The presented error analysis illustrates the efficiency of the proposed estimation.

For MDOF controlled structures, the suggested method is generalized by transforming the governing equations into a modal space. In this regard, a new formulation for the weighting matrices is provided based on a combination of optimal regulating parameters relative to each single mode. The numerical examples show the robustness of the proposed method for a variety of controlled shear-type buildings. In all cases, by applying the authors' control algorithm, a considerable decrease in structural responses is observed in comparison with other techniques.

References

Akhiev, S.S., Aldemir, U. and Bakioglu, M. (2002), "Multipoint instantaneous optimal control of structures", *Comput. Struct.*, **80**(11), 909-917.

Alavinasab, A., Moharrami, H. and Khajepour, A. (2006), "Active control of structures using energy-based LQR method", *Comput.-Aided Civil Infrastruct. Eng.*, **21**(8), 605-611.

Aldemir, U. (2009), "Evaluation of disturbance weighting parameter of minimax attenuation problems", *Comput.-Aided Civil Infrastruct. Eng.*, **24**(4), 302-308.

Aldemir, U. and Bakioglu, M. (2001), "Active structural control based on the prediction and degree of stability", *J. Sound Vib.*, **247**(4), 561-576.

Aldemir, U., Bakioglu, M. and Akhiev, S.S. (2001), "Optimal control of linear buildings under seismic excitations", *Earthq. Eng. Struct. D.*, **30**(6), 835-851.

Aldemir, U., Yanik, A. and Bakioglu, M. (2012), "Control of structural response under earthquake excitation", *Comput.-Aided Civil Infrastruct. Eng.*, **27**(8), 620-638.

Amini, F., Hazaveh, N.K. and Rad, A.A. (2013), "Wavelet PSO-based LQR algorithm for optimal structural control using active tuned mass dampers", *Comput.-Aided Civil Infrastruct. Eng.*, **28**(7), 542-557.

Amini, F. and Samani, M.Z. (2014), "A wavelet-based adaptive pole assignment method for structural control", *Comput. -Aided Civil Infrastruct. Eng.*, **29**(6), 464-477.

Amini, F. and Vahdani, R. (2008), "Fuzzy optimal control of uncertain dynamic characteristics in tall buildings subjected to seismic excitation", *J. Vib. Control*, **14**(12), 1843-1867.

Anderson, B.D.O. and Moore, J.B. (1989), Optimal Control:

Linear Quadratic Methods, Prentice Hall, Eaglewood Cliffs, New Jersey.

Assimakis, N.D., Lainiotis, D.G., Katsikas, S.K. and Sanida, F.L. (1997), "A survey of recursive algorithms for the solution of the discrete time Riccati equation", *Nonlinear Anal. Theory, Methods Appl.*, **30**(4), 2409-2420.

Bahar, O., Banan, M.R., Mahzoon, M. and Kitagawa, Y. (2003), "Instantaneous optimal wilson-θ control method", *J. Eng. Mech. - ASCE*, **129**(11), 1268-1276.

Bakioglu, M. and Aldemir, U. (2001), "A new numerical algorithm for sub-optimal control of earthquake excited linear structures", *Int. J. Numer. Meth. Eng*., **50**(12), 2601-2616.

Bani-Hani, K. and Ghaboussi, J. (1998), "Neural networks for structural control of a benchmark problem, active tendon system", *Earthq. Eng. Struct. D*., **27**(11), 1225-1246.

Barbosa, F.S. and Battista, R.C. (2007), "A numerical tool for solving Riccati equation applied to modal optimal control of structures", *Struct. Control Health Monit*., **14**(6), 915-930.

Braz-César, M.T. and Barros, R. (2018), "Semi-active fuzzy based control system for vibration reduction of a SDOF structure under seismic excitation", *Smart Struct. Syst*., **21**(4), 389-395.

Cao, H. and Li, Q.S. (2004), "New control strategies for active tuned mass damper systems", *Comput. Struct*., **82**(27), 2341-2350.

Chang, S., Kim, D., Kim, D.H. and Kang, K.W. (2012), "Earthquake response reduction of building structures using learning-based lattice pattern active controller", *J. Earthq. Eng.*, **16**(3), 317-328.

Chase, J.G. and Smith, H.A. (1996), "Robust H∞ control considering actuator saturation. I: theory", *J. Eng. Mech. - ASCE*, **122**(10), 976-983.

Cheng, F.Y., Jiang, H. and Lou, K. (2010), Smart Structures: Innovative Systems for Seismic Response Control, CRC Press, New York, USA.

Choi, C.H. (1990), "A survey of numerical methods for solving matrix Riccati differential equations", Southeastcon'90. Proceedings., IEEE.

Chung, L.L., Lin, C.C. and Lu, K.H. (1995), "Time-delay control of structures", *Earthq. Eng. Struct. D*., **24**(5), 687-701.

Datta, T.K. (2003), "A state-of-the-art review on active control of structures", *ISET J. Earthq. Technol*., **40**(1), 1-17.

Davison, E.J. and Maki, M.C. (1973), "The numerical solution of the matrix Riccati differential equation", *IEEE T. Autom. Control*, **18**(1), 71-73.

de Souza, L.C.G. (2006), "Design of satellite control system using optimal nonlinear theory", *Mech. Based Des. Struct*., **34**(4), 351-364.

Fisco, N.R. and Adeli, H. (2011), "Smart structures: Part I—Active and semi-active control", *Scientia Iranica, Transaction A: Civil Eng*., **18**(3), 275-284.

Fisco, N.R. and Adeli, H. (2011), "Smart structures: Part II—Hybrid control systems and control strategies", *Scientia Iranica, Transaction A: Civil Eng.*, **18**(3), 285-295.

Fu, T.S. and Johnson, E.A. (2017), "Semiactive control for a distributed mass damper system", *Struct. Control Health Monit.*, **24**(4), e1888.

Gluck, N., Reinhorn, A.M., Gluck, J. and Levy, R. (1996), "Design of supplemental dampers for control of structures", *J. Struct. Eng. - ASCE*, **122**(12), 1394-1399.

Guoping, C. and Jinzhi, H. (2002), "Optimal control method for seismically excited building structures with time-delay in control", *J. Eng. Mech. - ASCE*, **128**(6), 602-612.

Hashemi, S.M.A., Haji Kazemi, H. and Karamodin, A. (2016), "Localized genetically optimized wavelet neural network for semi-active control of buildings subjected to earthquake", *Struct. Control Health Monit*., **23**(8), 1074-1087.

Jang, D.D., Jung, H.J. and Moon, Y.J. (2014), "Active mass damper system using time delay control algorithm for building structure with unknown dynamics", *Smart Struct. Syst*., **13**(2), 305-318.

Kim, S.B. and Yun, C.B. (2000), "Sliding mode fuzzy control: Theory and verification on a benchmark structure", *Earthq. Eng. Struct. D.*, **29**(11), 1587-1608.

Korkmaz, S. (2011), "A review of active structural control: challenges for engineering informatics", *Comput. Struct*., **89**(23), 2113-2132.

Lee, J.D., Shen, S., Manzari, M.T. and Shen, Y.L. (2008), "Structural control algorithms in earthquake resistant design", *J. Earthq. Eng*., **4**(1), 67-96.

Lee, S.H., Min, K.W., Hwang, J.S. and Kim, J. (2004), "Evaluation of equivalent damping ratio of a structure with added dampers", *Eng. Struct*., **26**(3), 335-346.

Li, Z. and Adeli, H. (2016), "New discrete-time robust H2/H∞ algorithm for vibration control of smart structures using linear matrix inequalities", *Eng. Appl. Artif. Intel*., **55**, 47-57.

Lu, L.T., Chiang, W.L. and Tang, J.P. (1998), "LQG/LTR control methodology in active structural control", *J. Eng. Mech. - ASCE*, **124**(4), 446-454.

Lynch, J.P. and Law, K.H. (2002), "Market-based control of linear structural systems", *Earthq. Eng. Struct. D*., **31**(10), 1855-1877.

Ma, T.W. and Yang, H.T.Y. (2004), "Adaptive feedback-feedforward control of building structures", *J. Eng. Mech. - ASCE*, **130**(7), 786-793.

Marco, A., Hennig, P., Bohg, J., Schaal, S. and Trimpe, S. (2016), "Automatic LQR tuning based on Gaussian process global optimization", *Proceedings of the International Conference on Robotics and Automation (ICRA 2016)*, IEEE.

Mariani, C. and Venini, P. (1998), "On the use of stochastic models of uncertainty in active control and structural optimization", *Comput. Struct*., **67**(1), 105-117.

Materazzi, A.L. and Ubertini, F. (2012), "Robust structural control with system constraints", *Struct. Control Health Monit*., **19**(3), 472-490.

Miller, R.K., Masri, S.F., Dehghanyar, T.J. and Caughey, T.K. (1988), "Active vibration control of large civil structures", *J. Eng. Mech. - ASCE*, **114**(9), 1542-1570.

Min, K.W., Hwang, J.S., Lee, S.H. and Chung, L. (2003), "Probabilistic approach for active control based on structural energy", *Earthq. Eng. Struct. D.*, **32**(15), 2301-2318.

Miyamoto, K., She, J., Imani, J., Xin, X. and Sato, D. (2016), "Equivalent-input-disturbance approach to active structural control for seismically excited buildings", *Eng. Struct*., **125**, 392-399.

Miyamoto, K., She, J., Sato, D. and Yasuo, N. (2018), "Automatic determination of LQR weighting matrices for active structural control", *Eng. Struct*., **174**, 308-321.

Morales-Beltran, M. and Paul, J. (2015), "Technical note: active and semi-active strategies to control building structures under large earthquake motion", *J. Earthq. Eng*., **19**(7), 1086-1111.

Nguyen, T.A. and Bestle, D. (2007), "Application of optimization methods to controller design for active suspensions", *Mech. Based Des. Struct*., **35**(3), 291-318.

Ohtori, Y., Christenson, R.E., Spencer Jr., B.F. and Dyke, S.J. (2004), "Benchmark control problems for seismically excited nonlinear buildings", *J. Eng. Mech. - ASCE*, **130**(4), 366-385.

Park, K.S. and Ok, S.Y. (2015), "Modal-space reference-model-tracking fuzzy control of earthquake excited structures", *J. Sound Vib*., **334**, 136-150.

Pnevmatikos, N.G. and Gantes, C.J. (2011), "Influence of time delay and saturation capacity to the response of controlled structures under earthquake excitations", *Smart Struct. Syst*., **8**(5), 449-470.

Reinhorn, A.M., Lavan, O. and Cimellaro, G.P. (2009), "Design of controlled elastic and inelastic structures", *Earthq. Eng. Eng.*

Vib., **8**(4), 469-479.

Reinhorn, A.M., Soong, T.T., Riley, M.A., Lin, R.C., Aizawa, S. and Higashino, M. (1993), "Full-scale implementation of active control. II: Installation and performance", *J. Struct. Eng. - ASCE*, **119**(6), 1935-1960.

Sajeeb, R., Manohar, C.S. and Roy, D. (2007), "Use of particle filters in an active control algorithm for noisy nonlinear structural dynamical systems", *J. Sound Vib*., **306**(1), 111-135.

Schmitendorf, W.E., Jabbari, F. and Yang, J.N. (1994), "Robust control techniques for buildings under earthquake excitation", *Earthq. Eng. Struct. D*., **23**(5), 539-552.

Shukla, P., Ghodki, D., Manjarekar, N.S. and Singru, P.M. (2016), "A Study of H infinity and H2 synthesis for active vibration control", *IFAC-PapersOnLine*, **49**(1), 623-628.

Singh, M.P., Matheu, E.E. and Suarez, L.E. (1997), "Active and semi-active control of structures under seismic excitation", *Earthq. Eng. Struct. D*., **26**(2), 193-213.

Song, G., Lin, J., Williams, F.W. and Wu, Z. (2006), "Precise integration strategy for aseismic LQG control of structures", Int. *Int. J. Numer. Meth. Eng*., **68**(12), 1281-1300.

Soong, T.T. (1988), "State-of-the-art review: Active structural control in civil engineering", *Eng. Struct*., **10**(2), 74-84.

Soong, T.T., Reinhorn, A.M., Wang, Y.P. and Lin, R.C. (1991), "Full-scale implementation of active control. I: Design and simulation", *J. Struct. Eng. - ASCE*, **117**(11), 3516-3536.

Soong, T.T. and Spencer Jr., B.F. (2000), "Active, semi-active and hybrid control of structures", *Bull. New Zealand National Soc. Earthq. Eng*., **33**(3), 387-402.

Spencer Jr., B.F. and Nagarajaiah, S. (2003), "State of the art of structural control", *J. Struct. Eng. - ASCE*, **129**(7), 845-856.

Spencer Jr., B.F. and Sain, M.K. (1997), "Controlling buildings: a new frontier in feedback", *IEEE Control Syst. Mag. Emerg. Technol*., **17**(6), 19-35.

Symans, M.D. and Constantinou, M.C. (1999), "Semi-active control systems for seismic protection of structures: a state-of-the-art review", *Eng. Struct*., **21**(6), 469-487.

Tarantino, J., Bruch Jr., J.C. and Sloss, J.M. (2004), "Instantaneous optimal control of seismically-excited structures using a maximum principle", *J. Vib. Control*, **10**(8), 1099-1121.

Teng, J., Xing, H.B., Lu, W., Li, Z.H. and Chen, C.J. (2016), "Influence analysis of time delay to active mass damper control system using pole assignment method", *Mech. Syst. Signal Pr*., **80**, 99-116.

Wang, N. and Adeli, H. (2015), "Self-constructing wavelet neural network algorithm for nonlinear control of large structures", *Eng. Appl. Artif. Intel*., **41**, 249-258.

Wang, S.G. (2003), "Robust active control for uncertain structural systems with acceleration sensors", *J. Struct. Control*, **10**(1), 59-76.

Wang, Z., Chen, S. and Han, W. (1999), "Integrated structural and control optimization of intelligent structures", *Eng. Struct.*, **21**(2), 183-191.

Wong, K.K.F. and Hart, G.C. (1997), "Active control of inelastic structural response during earthquakes", *Struct. Des. Tall Build*., **6**(2), 125-149.

Wong, K.K.F. and Yang, R. (2001), "Effectiveness of structural control based on control energy perspectives", *Earthq. Eng. Struct. D.*, **30**(12), 1747-1768.

Xing, L., Tachibana, E. and Inoue, Y. (2000), "QN control method for building vibration caused by periodic excitation acting on intermediate story", *Earthq. Eng. Struct. D*., **29**(8), 1079-1091.

Xu, J.Y., Tang, J. and Li, Q.S. (2002), "An efficient method for the solution of Riccati equation in structural control implementation", *Appl. Acoust.*, **63**(11), 1215-1232.

Yamada, K. and Kobori, T. (2001), "Fundamental dynamics and control strategies for aseismic structural control", *Int. J. Solids Struct*., **38**(34), 6079-6121.

Yang, J.N., Lin, S. and Jabbari, F. (2003), "H2-based control strategies for civil engineering structures", *J. Struct. Control*, **10**(3-4), 205-230.

HJ